Hindawi
Shock and Vibration
Volume 2020, Article ID 5602917, 13 pages
https://doi.org/10.1155/2020/5602917

Research Article

Sliding Mode Control of Vehicle Equipped with Brake-by-Wire System considering Braking Comfort

Shuai Chen, Xilong Zhang, and Jizhong Wang

School of Mechanical and Automotive Engineering, Qingdao University of Technology, Qingdao 266520, China

Correspondence should be addressed to Xilong Zhang; 135078809@qq.com

Received 2 July 2019; Revised 3 September 2019; Accepted 19 September 2019; Published 25 February 2020

Academic Editor: Dr Mahdi Mohammadpour

For passengers, the most common feeling during running on the bumpy road is continuous vertical discomfort, and when the vehicle is braking, especially the emergency braking, the instantaneous inertia of the vehicle can also cause a strong discomfort of the passengers, so studying the comfort of the vehicle during the braking process is of great significance for improving the performance of the vehicle. This paper presented a complete control scheme for vehicles equipped with the brake-by-wire (BBW) system aiming at ensuring braking comfort. A novel braking intention classification method was proposed based on vehicle braking comfort, which divided braking intention into mild brake, medium comfort brake, and emergency brake. Correspondingly, in order to improve the control accuracy of the vehicle brake system and to best meet the driver's brake needs, a braking intention recognizer relying on fuzzy logic was established, which used the road condition and the brake pedal voltage and its change rate as input, output real-time driver's braking intention, and braking intensity. An optimal brake force distribution strategy for the vehicle equipped with the BBW system based on slip rate was proposed to determine the relationship between braking intensity and target slip ratio. Combined with the vehicle dynamics model, improved sliding mode controller, and brake force observer, the joint simulation was conducted in Simulink and CarSim. The cosimulation results show that the proposed braking intention classification method, braking intention recognizer, brake force distribution strategy, and sliding mode control can well ensure the braking comfort of the vehicle equipped with the BBW system under the premise of ensuring brake safety.

1. Introduction

Ride comfort is an important factor for the design of autonomous vehicles and intelligent transportation systems. At the same time, ride comfort is affected by various factors, for example, vibration, sound, temperature, visual stimuli, and vehicle structure design. A great number of research studies have been conducted to improving ride comfort, particularly in the field concerning ride uncomfortable feeling caused by vertical vibration, and a great deal of active and passive suspension control algorithms was put forward to improve the vertical vibration [1, 2]. However, the discomfort feeling is not only derived from the vertical vibration, but it is also caused by amount of vehicle acceleration and jerk in the longitudinal direction, which is the amount of change in vehicle acceleration [3]; this situation is very common when the vehicle is accelerating or decelerating. Nonetheless, there is still little research on this subject. So, we only concern one of the factors that influenced ride comfort in this paper, which is related to vehicle longitudinal dynamics. In the mean time, with the development of electronic control technology, the type of brake system is also changing. As the future form of the brake system, the mechanical links between the brake pedal and the brake actuator are eliminated in the BBW system, which are substituted by electronic signals and control units. Therefore, the BBW system has the characteristics of efficient and steady brake response, which is easy to integrate the advantages of other functional modules [4]. This advantage also lays the structure foundation for improving vehicle safety and ride comfort.

Many scholars have paid more attention to the control algorithm of the BBW system for the brake performance of the vehicle, such as slip rate and braking distance. Haggag and Abidou [5] developed an optimal control tracking

strategy for a BBW system and tested on a laboratory setup consisting of a driving motor, an electromechanical brake actuator, and other related hardware. Chen et al. [6] proposed an antilock braking control algorithm of direct slip rate based on the hybrid brake system with the electrohydraulic brake (EHB) equipped on the front wheels and the electromechanical brake (EMB) equipped on the rear wheels. Wang et al. [7] proposed the sliding model controller to effectively control the dc motor in the BBW system, which can effectively improve the emergency braking performance in the typical simulation manoeuvre employed and significantly reduced the tracking errors.

Despite the BBW system has the structure advantage, it also requires some precise and reliable control algorithms to ensure the ride comfort concerning the area of longitudinal vibration. Due to the continuous sudden acceleration or deceleration of the vehicle, the passenger and the vehicle body will receive the inertia force which can cause physical discomfort, along with the change of road condition and driver intention; this feeling of discomfort will be exacerbated. The braking comfort means ride comfort when the vehicle is braking, though the research in ride comfort had start long-time back and still growing, but no final word has been said, which opens the way to more active and creative research [8]. Thus, we take the braking deceleration as the main assessment criteria in this paper. Studies have shown that vehicles with accelerations greater than 0.5 g can cause discomfort feeling when braking, and brake deceleration of vehicles less than 0.5 g is acceptable when the normal brake is applied [9]. The maximum deceleration of the vehicle when the emergency brake is applied is generally 0.75 g to 0.85 g [10]. For this purpose, some researchers have also made corresponding braking comfort studies: Pan et al. [11] proposed an antilock braking control strategy considering the comfort of the coordinated braking system of the distributed driven electric vehicle, and the control strategy has obtained the great braking comfort performance by decreasing the hydraulic pressure modulation, solenoid valve actuation, and the brake pedal stroke. Zong et al. [12] developed a control strategy of the electronic braking system which focused on the comfort assessment of the vehicle, and this strategy can select the maximum deceleration according to the road condition and the comfortable feeling of the driver. Zheng et al. [13] presented a control method with a three-layer hierarchical structure aiming at improving the vehicle braking comfort, and the third layer of the structure includes a braking force distribution control method which could control the vehicle deceleration with a smooth axle load transfer process based on linear matrix inequality. Soltani et al. [14] proposed a coordinated control of the semiactive suspension and the active braking using a fuzzy controller and an adaptive sliding mode controller, and the simulation results show that this strategy could effectively improve the vehicle handling, stability, and ride comfort.

Based on the above analysis, most of previous studies of the vehicle equipped with the BBW system focused on the brake actuator and controller strategy of emergency braking; only few studies were conducted to ensuring the braking comfort vehicle equipped with the BBW system. In other words, no matter which kind of braking is applied, the vehicle comfort all need to be considered, and the human-vehicle-road closed-loop control system was rarely mentioned in previous research; hence, there is still a lot of room for improvement in this aspect. Considering the importance of the road condition and driver's intention, the main purpose of this paper is to study the sliding mode control of the vehicle equipped with the BBW system for ensuring braking comfort under the condition of braking intentions and road surface changing while ensuring vehicle safety; the systematic control flowchart is shown in Figure 1.

The rest of the paper is divided into 4 sections: Section 2 introduces the braking intention classification method considering the braking comfort, and the braking intention recognizer is designed by fuzzy logic to identify the driver's braking intention and braking intensity in real time. The model of the vehicle and the BBW system are given, and an optimal brake force allocation strategy based on the slip rate for the vehicle equipped with the BBW system is proposed in Section 3. Section 4 demonstrates cosimulation results and analysis of Simulink and CarSim. Finally, conclusion is given in Section 5.

2. Braking Intention

2.1. Braking Intention Classification. Nowadays, the classification study of braking intentions is not at all the same criteria due to the different research directions of researchers. However, the classification method of braking intention has a positive effect on improving the running performance of the vehicle, so it is necessary to select a reasonable and effective braking intention classification method dealing with the complicated control problem. In this paper, considering the problem of braking comfort of the vehicle equipped with the BBW system and driver's actual operation process during the running of the vehicle, the braking intention is divided into mild brake, medium comfort brake, and emergency brake.

During the running of the vehicle, when the driver finds there is an obstacle or an intersection in the front, it is necessary to perform a deceleration action, and then the speed is immediately increased after the deceleration, and this situation is called mild brake; the vehicle only experienced a slight deceleration in this condition, which did not cause too much discomfort to the passenger on the vehicle. When the driver finds a red light in front of a relatively far distance or when parking is needed farther in front, the driver will perform a series of brake parking actions, which is called medium comfort brake. Passengers will have a greater sense of discomfort compared with mild brake; thus, this condition needs to be properly regulated. There is also a case where the driver needs to make an emergency avoidance when there is another sudden situation such as a vehicle or a pedestrian in a small distance ahead, and the driver needs to take an action to quickly stop, which is called emergency brake. Due to the inertia and the axial load transfer, the passenger discomfort during the emergency brake process is the strongest. Therefore, during the brake process, the vehicle should perform the brake action in real time in

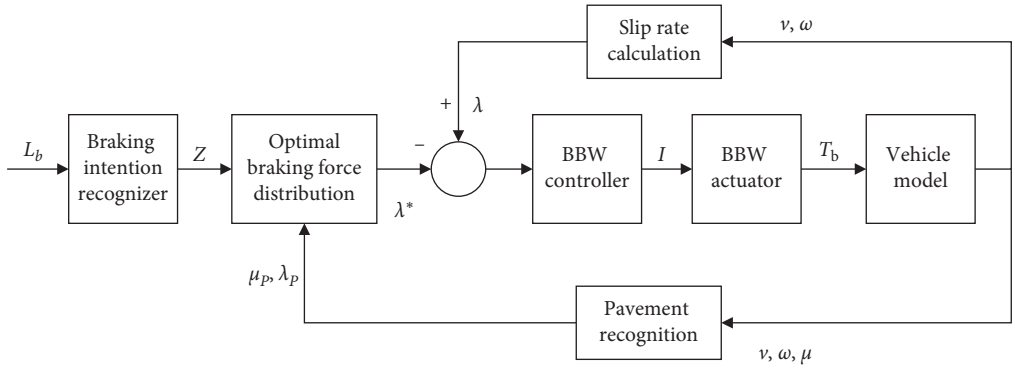

Figure 1: Control structure of the BBW system considering braking comfort. L_b is brake pedal opening, Z is output brake intensity, μ_p is current road peak adhesion coefficient, λ_p is current road optimal slip rate, λ^* is current desired slip rate, λ is actual slip rate, I is drive motor armature current, T_b is brake disc output torque, v is vehicle longitudinal speed, ω is angular velocity of wheel rotation, and μ is brake force coefficient.

accordance with the driver's intention, and the braking comfort should be considered while ensuring the safety of the brake.

2.2. Braking Intention Recognizer. According to the feature of the braking intention classification, the intention recognizer is needed to output the desired driver's intention and the corresponding braking intensity. The brake pedal angular displacement and its change rate can reflect the driver's braking intention, in view of the actual engineering brake pedal angular displacement, and its change rate will be expressed by the output voltage of the brake pedal and its change rate. Therefore, the electronic brake pedal data acquisition system was built based on the microcontroller (STM32F103ZET6) which could provide accurate data collection function. The data acquisition system comprises four parts: electronic brake pedal, ADC chip (ADS1212), mircrocontroller (STM32F103ZET6), and upper computer. The ADC chip collects the output voltage and the angular displacement of the electric brake pedal, respectively, and transfers it to mircrocontroller through SPI protocol, and then the upper computer can get the data from the mircrocontroller. Hence, the data acquisition system could reflect the relationship of pedal angular displacement and the output voltage. The output voltage of the electronic brake pedal varies from 0 V to 5 V, and the angular displacement varies from 0° to 20°. Figure 2 shows the relationship between the angular displacement of the brake pedal and the output voltage. As is shown in Figure 2, the pedal output voltage changes with pedal angular displacement in a linear relationship, and then the relationship between the pedal angular displacement and the output voltage is calibrated by data fitting, and the formula is given in the following equation:

$$U = 0.306\theta - 0.7097, \quad (1)$$

where U is the output voltage of the electronic brake pedal and θ is the angular displacement of the brake pedal.

Since the relationship between braking intention and braking intensity is related to the change of the road surface; in order to improve the control precision of the brake system, the road condition is also taken into account when designing the braking intention recognizer. So, the road condition, output voltage, and its change rate are used as input parameters of the intention recognizer, and the output parameters are the braking intention and the corresponding braking intensity. Figure 3 shows the structure of a braking intention recognizer.

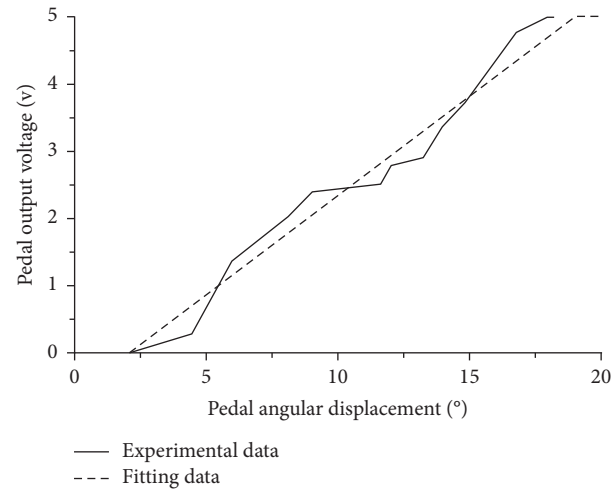

Figure 2: Fit curve of pedal angular displacement and pedal output voltage.

As is shown in Figure 3, the output braking intention is acquired by the output voltage and its change rate, and then it will become the input parameters together with road condition to determine the output intensity, and we only take the dry asphalt, wet asphalt, and snow-covered road surface into account in this paper. The braking intention recognizer is built based on fuzzy logic, and the input and output variables of fuzzy logic need to be blurred. Therefore, the domain of output voltage is defined as [0, 5], and its fuzzy language is described as [zero (Z), small (S), medium (M), big (B)]. The domain of the change rate of output voltage is defined as [0, 60], and its fuzzy language is described as [zero

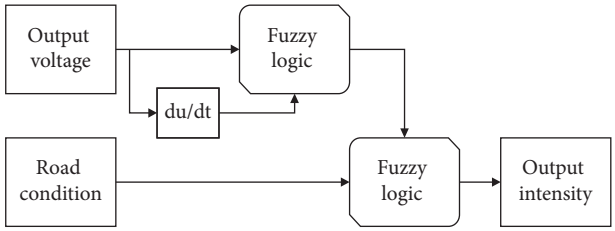

Figure 3: The structure of the braking intention recognizer.

(Z), small (S), medium (M), big (B)]. The membership function about output voltage and its change rate are shown in Figure 4.

The domain of the output braking intention is defined as [0, 3], and its fuzzy language is described as [zero (Z), small (S), medium (M), emergency (E)]. The domain of the input braking intention is defined as [0, 3], and its fuzzy language is described as [zero (Z), small (S), medium (M), emergency (E)]. The membership function about output and input braking intention is shown in Figure 5.

The domain of the road condition is defined as [0, 3], and its fuzzy language is described as [dry asphalt (D), wet asphalt (W), ice-snow (I)]. The domain of the braking intensity is [0, 1], and its fuzzy language is described as [zero (Z), small (S), medium (M), big (B)]. The membership function about the road condition and braking intensity are shown in Figure 6.

The triangular and trapezoid shapes (as shown in Figures 4–6) are selected for the membership functions of inputs and outputs. According to the above characteristics of input variables and output variables, the fuzzy inference rules for braking intention recognition and braking intensity identification are designed [15]. Hence, the intention recognizer could output the driver's intention and intensity in the real time which is beneficial for the control to absorbing the longitudinal vibration.

3. Model of the Vehicle Equipped with the Brake-by-Wire System

3.1. Vehicle Dynamic Model. A Sedan is selected as the research object. In order to simplify the analysis of the problem, the following assumptions are made on the vehicle model:

(i) The air resistance and rolling resistance moment are not considered when the vehicle is running

(ii) The inertia resistance moment generated when the vehicle rotating parts decelerated is not considered

(iii) Inconsistent vertical load of the left and right wheels caused by roll is not considered, that is, only the longitudinal force of the vehicle is considered in this model

(iv) Assuming that the wheels of the vehicle are in good contact with the flat road surface

The vehicle longitudinal dynamic equation is described as follows [16]:

$$m\dot{v} = \sum_{i=1}^{4} F_{xi}. \tag{2}$$

The tire dynamics equation is described as follows [16]:

$$J_i\dot{\omega}_i = r_i F_{xi} - T_{bi}. \tag{3}$$

Wheel slip ratio equation is described as follows [16]:

$$\lambda_i = \frac{v - \omega_i r_i}{v}, \tag{4}$$

where $i = 1, 2, 3$, and 4 represents the left-front wheel, right-front wheel, left-rear wheel, and right-rear wheel of the vehicle, respectively, m is the vehicle mass, F_{xi} represents the wheel longitudinal ground brake force with the serial number i, $\dot{v}$ represents the vehicle longitudinal acceleration, J is the moment of inertia of the wheel, $\dot{\omega}$ is the angular acceleration of wheel rotation, and r is the wheel rolling radius. T_b is the wheel braking torque, and v is the vehicle longitudinal speed.

3.2. Pavement Recognition Model. The same pedal angle could produce different braking intensities on road surfaces with different adhesion coefficients, that is, the same braking intensity could produce different braking decelerations on different road surfaces, resulting in different braking performances of the vehicle. The road surface recognition has a greater impact on vehicle braking; thus, when the road surface adhesion coefficient changes, the brake intention recognizer should accurately and timely reflect the driver's braking intention. In this paper, when the vehicle is braking, the slip rate and the real-time braking force coefficient will be calculated, respectively, while the standard braking force coefficient of seven different road surfaces could be obtained by the Burckhardt tire model [17]; the standard braking force coefficient $\mu(\lambda)$ [17] is described as equation (5), and the relationship between standard braking force coefficient and wheel slip rate is given by Figure 7. Then, the type of road surface can be determined in real time by doing difference of standard and real-time braking force coefficient under the condition of the same slip rate, and the real-time braking force coefficient is described as

$$\mu(\lambda) = c_1\left(1 - e^{-c_2\lambda}\right) - c_3\lambda, \tag{5}$$

$$\widehat{\mu}_i = \frac{F_{xi}}{F_{zi}}, \tag{6}$$

where C_1, C_2, and C_3, respectively, are the model fitting parameters [17], and their value changes with the state of the road surface. We use three sets of road arguments of C_1, C_2, and C_3, and the value is shown in Table 1. $\widehat{\mu}_i$ is the observed value (real-time) of braking force coefficient. F_{zi} represents the vertical load of each wheel; because the wheel vertical load has a great influence on the process of braking, we can use equation (7) to estimate the vertical load of front and rear axle:

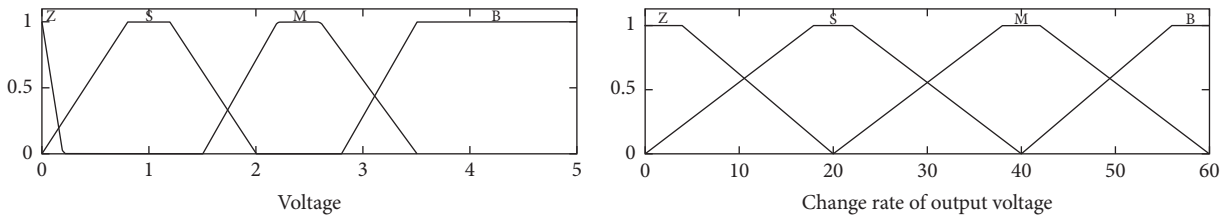

Figure 4: The membership function about output voltage and its change rate.

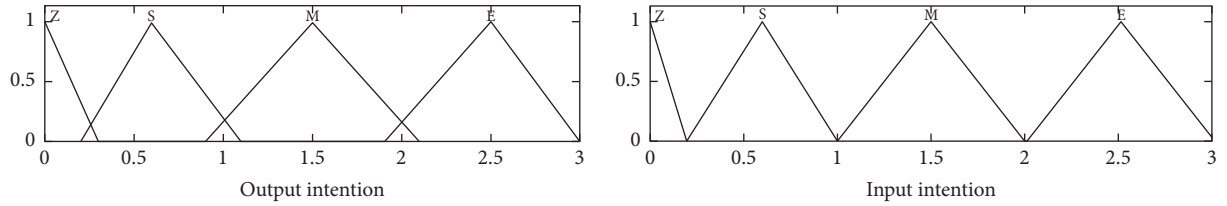

Figure 5: The membership function about output and input braking intention.

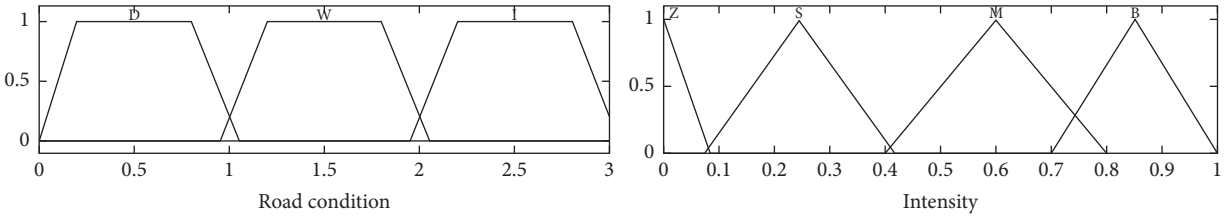

Figure 6: The membership function about the road condition and braking intensity.

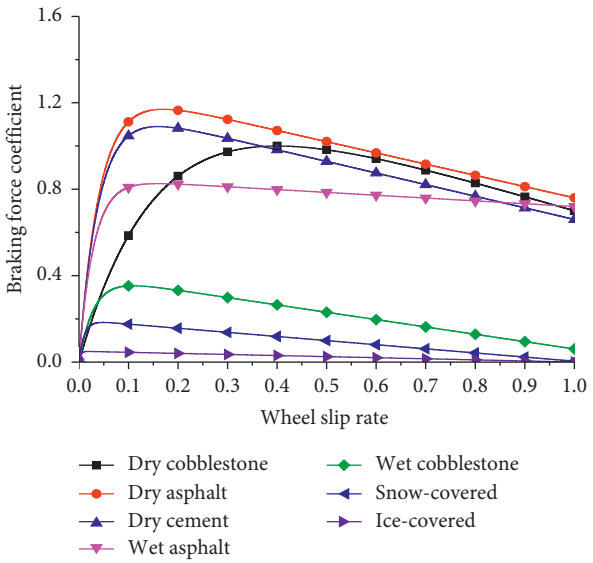

Figure 7: The relationship between braking force coefficient and wheel slip rate.

Table 1: The value of C_1, C_2, and C_3.

The type of road	C_1	C_2	C_3
Dry asphalt road	1.2801	23.99	0.52
Wet asphalt road	0.8570	33.822	0.347
Snow-covered road	0.1946	94.129	0.0646

$$
\begin{aligned}
F_{z1} &= \frac{1}{2L}\left(mgb + m_s h_s \dot{v} + h_{us}\dot{v}\left(m_{us} + \frac{I_f}{r_1^2} + \frac{I_r}{r_1^2}\right)\right),\\
F_{z2} &= \frac{1}{2L}\left(mgb + m_s h_s \dot{v} + h_{us}\dot{v}\left(m_{us} + \frac{I_f}{r_2^2} + \frac{I_r}{r_2^2}\right)\right),\\
F_{z3} &= \frac{1}{2L}\left(mga - m_s h_s \dot{v} - h_{us}\dot{v}\left(m_{us} + \frac{I_f}{r_3^2} + \frac{I_r}{r_3^2}\right)\right),\\
F_{z4} &= \frac{1}{2L}\left(mga - m_s h_s \dot{v} - h_{us}\dot{v}\left(m_{us} + \frac{I_f}{r_4^2} + \frac{I_r}{r_4^2}\right)\right).
\end{aligned} \tag{7}
$$

3.3. Brake-by-Wire System Model. BBW system mainly has two types of actuator, that is, EHB and EMB. EHB still retains the conventional hydraulic brake parts at the vehicle, which are different with EMB. Thus, EMB is the real brake-by-wire in the full sense; because the actuator of EMB is the drive motor which receives the control signal from the control unit, it means it puts forward the higher requirements to the design of the braking system. In this paper, the research object is an EMB actuator; a floating front disc brake is used, which includes a drive motor, a planetary gear, a ball screw, and a brake disc. The driving motor could provide the original electromagnetic torque to the planetary gear, as the reduction mechanism, the planetary gear transfers torque to the screw, and then the ball screw

converts the rotary motion of the planetary gear shaft into the linear motion of the screw nut and exerts pressure on the brake disc through the brake pad; therefore, the brake disc could output the brake torque. The schematic diagram of the BBW system actuator is shown in Figure 8.

The braking torque of the entire brake system is given as follows:

$$T_{bi} = \begin{cases} 0, & |T_{ei}| \le T_{fi}, \\ k_{bi}\left(k_{ti} I_i - T_{fi}\right), & |T_{ei}| > T_{fi}, \end{cases} \tag{8}$$

$$k_{bi} = \frac{4\pi \mu_{bi} r_{bi} \eta_{si} i_{xi} \eta_{xi}}{p_{hi}},$$

where T_e is the drive motor electromagnetic torque, T_f is the drive motor friction torque, I is the drive motor armature current, k_b is the brake output torque coefficient, k_t is the motor torque coefficient of the brake, μ_b is the brake pad friction coefficient, r_b is the brake disc radius, η_s is the mechanical efficiency of the ball screw, i_x is the planetary gear ratio, η_x is the mechanical efficiency of the planetary gear mechanism, and p_h is the lead of the screw. T_b is the wheel braking torque.

3.4. Optimal Braking Force Distribution Strategy. During the braking process of the vehicle, side slip phenomenon may occur if the rear wheel is locked before the front wheel, which is a very dangerous situation. Therefore, in order to improve the braking comfort under the premise of ensuring the safety of braking, this paper proposed a braking force distribution strategy based on the optimal slip ratio, that is, in addition to emergency braking, the slip rate of each wheel is controlled to be kept at a small value during vehicle braking, and the front wheel slip ratio is controlled to be greater than the rear wheel slip ratio so that to keep the vehicle's brake deceleration rate change in a gentle state. In emergency braking, the target slip ratio of the four wheels is simultaneously set to the current optimum slip ratio of the road surface. This strategy calculates the longitudinal braking force of the tire in real time in combination with the Burckhardt tire model. So, the distribution strategy can be described by a quadratic programming problem with inequality constraints which could be solved by the active set method. The mathematical model is given as follows:

$$\begin{aligned} \min \quad & f = {\lambda_f}^2 + {\lambda_r}^2, \\ \text{s.t.} \quad & \lambda_f > \lambda_r, \\ & \sum_{i=1}^{4} F_{xi} = mgZ, \\ & 0 \le \lambda_f, \lambda_r \le 1, \end{aligned} \tag{9}$$

where λ_f, λ_r is the slip ratio of the front and rear axle, respectively.

3.5. Sliding Mode Controller. In view of the high nonlinearity and uncertainty in the process of automobile braking, the sliding mode variable structure control has superior control effect, but its shortcoming is that the chattering effect is generated during the control process, which affects the system control precision. Therefore, the improved exponential rate is adopted in this paper. The sliding mode variable structure controller can reduce the influence of the chattering effect and ensure the robustness of the sliding mode control.

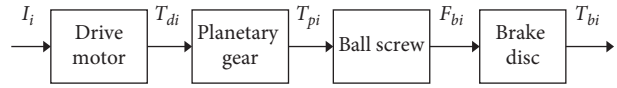

Figure 8: The schematic diagram of the BBW system actuator. I_i is the drive motor armature current, T_{di} is the motor output torque, T_{pi} is the planetary gear output torque, F_{bi} is the brake pad pressure on the brake disc, and T_{bi} is the brake disc output torque.

Firstly, switching function is selected using the bias of current-desired slip ratio λ^* and actual slip ratio λ, and the sliding surface s is described as

$$s = \lambda^* - \lambda. \tag{10}$$

When $\dot{s} = 0$, the equivalent control of the system I_{eqi} is described as follows:

$$I_{eqi} = \frac{r_i F_{xi}}{k_{bi} k_{ti}} + \frac{T_{fi}}{k_{ti}} + \frac{J_i \omega_i}{mvk_{bi} k_{ti}} \left(F_{x1} + F_{x2} + F_{x3} + F_{x4}\right). \tag{11}$$

The improved exponential rate function is derived as

$$I_{si} = -k_1 |s_i| \operatorname{sgn}(s_i) - k_2 s_i, \tag{12}$$

where $k_1 > 0$, $k_2 > 0$ is the variable speed approach law coefficient and exponential convergence law coefficient, respectively, which could influence the control speed and robustness of the control system. Equation (13) satisfies the arrival condition of the sliding mode variable structure control. The proof process is as follows:

$$\begin{aligned} s\dot{s} &= s\left(-k_1 |s| \operatorname{sgn}(s) - k_2 s\right) \\ &= -k_1 s|s| \frac{s}{|s|} - k_2 s^2 \\ &= -k_1 s^2 - k_2 s^2 \le 0. \end{aligned} \tag{13}$$

Therefore, the control system is stable, and the control law of the sliding mode controller is shown as

$$\begin{aligned} I_i = {} & \frac{J_i \omega_i}{mvk_{bi} k_{ti}} \left(F_{x1} + F_{x2} + F_{x3} + F_{x4}\right) + \frac{r_i F_{xi}}{k_{bi} k_{ti}} + \frac{T_{fi}}{k_{ti}} \\ & - k_1 |s_i| \operatorname{sgn}(s_i) - k_2 s_i \end{aligned} \tag{14}$$

The sliding mode controller is optimized through adjusting the variable speed approach law coefficient k_1 and exponential convergence law coefficient k_2. When the controlled variable is far away from the sliding mode surface,

k_2 plays an important role in this situation, and the state trajectory of the control system rapidly approaches the sliding mode surface in the exponential form. When the controlled variable approached the sliding mode surface, here, k_1 plays the important role, and the state trajectory of the control system will reach the steady state.

As the characteristic of the sliding mode control, the problem of chatter could influence the control accuracy of the brake system; hence, in order to solve this problem to improve the control accuracy, we choose to use the saturation function to replace the sign function, and the saturation function is described as

$$\text{sat}\left(\frac{s}{\varphi}\right) = \begin{cases} \dfrac{s}{\varphi}, & |s| \le \varphi, \\ \text{sgn}\left(\dfrac{s}{\varphi}\right), & |s| > \varphi, \end{cases} \tag{15}$$

where φ is the boundary layer.

4. Verification of the Control System Model

4.1. Structure of the Simulation Environment. CarSim [18] is simulation software designed for analyzing vehicle dynamics, developing active controllers, which is widely used in the automotive research and development. And it can deliver accurate, detailed, and efficient methods for simulating the performance of passenger vehicles. Simulink [19] is a block diagram design environment based on MATLAB, and it is a software package for the dynamic system model, simulation, and analysis. In order to, respectively, apply this control algorithm concerning braking comfort to a prototyping system and real-car experiment in the future, hence, according to actual experiment requirement, the braking intention recognizer and the improved sliding mode control algorithm are simulated in CarSim and Simulink in this paper.

D-class Sedan is selected as the research object in CarSim, and then the CarSim vehicle model is built. The vehicle braking system in CarSim is set as No dataset selected, and the braking control in the procedures is set as No dataset selected. The braking torque of each wheel is set in CarSim as the input variables of the vehicle model, and the vehicle speed, acceleration, and four-wheel angular rate are set as the output variables of the CarSim vehicle model. Then, the braking intention recognizer, the sliding mode controller, brake force distribution strategy model, EMB brake model, pavement recognition model, wheel slip rate calculation model, and wheel vertical load model are constructed in Simulink. The structure of the simulation environment is shown in Figure 9.

This paper designed two sets of simulation scenarios:

I (a) Medium comfort brake, switch dry asphalt pavement to wet asphalt pavement

I (b) Medium comfort brake, switch wet asphalt pavement to snow-covered pavement

II (a) Dry asphalt pavement, switch mild brake to medium comfort brake

II (b) Wet asphalt pavement, switch mild brake to medium comfort brake

In order to show the performance of the vehicle equipped with EMB, we could compare the vehicle equipped with ABS (ABS vehicle) with the vehicle equipped with EMB (EMB vehicle). The common simulation conditions are set as follows: the vehicle is running on a long straight road, which is no steering input during the simulation, and the initial longitudinal speed of the vehicle is 100 km/h. What need to be declared in advance is that the dry asphalt pavement and wet asphalt pavement's peak adhesion coefficient, respectively, are 1.17 and 0.8013, and the snow-covered pavement's peak adhesion coefficient is 0.1907 [17]. The wheel slip rate, vehicle acceleration, wheel braking torque, and vehicle speed are used to evaluate the performance of vehicle braking comfort in this paper.

4.2. Simulation Results

4.2.1. Scenario I (a) Medium Comfort Brake, Switch Dry Asphalt Pavement to Wet Asphalt Pavement. In the simulation scenarios, the driver conducts the medium comfort brake when $T = 0$ s, and the road surface changes from dry asphalt to wet asphalt at 15 meters, and the cosimulation results are shown in Figure 10.

As is descried above, brake deceleration of the vehicle less than 0.5 g is acceptable when the mild and medium comfort brake is applied. Figure 10 illustrates the vehicle longitudinal acceleration, speed, wheel slip rate, and brake torque, respectively, when the driver conducts the medium comfort brake on two different road surfaces. Because the change rule of four-wheel slip rate is the same, just taking the right-front wheel as an example, the wheel slip rate of the EMB vehicle is steadily controlled by the sliding model algorithm at a specified value no matter which kind of road surface the vehicle is on, while the wheel slip rate of the ABS vehicle could not follow the road optimal slip rate. The acceleration of the EMB vehicle suddenly increases to −0.58 g when the vehicle is on the dry asphalt pavement, which means it already has brought the mild discomfort feeling to the passenger. But, it decreases to −0.33 g when the road surface changes to wet asphalt pavement after 15 meters, which is acceptable to the passenger. However, the acceleration of the ABS vehicle on the dry asphalt road is near −0.65 g which is not acceptable, but it decreases to −0.45 g when the road surface changes, which is acceptable to the passenger. Thus, the feeling in the EMB vehicle is better than in the ABS vehicle under the condition of ensuring vehicle safety. The rear axel wheel brake torque of the EMB vehicle is maintained in 0 Nm no matter on which road surface, but the front axle brake torque plays an important part in the brake process, which is determined by braking force distribution.

4.2.2. Scenario I (b) Medium Comfort Brake, Switch Wet Asphalt Pavement to Snow-Covered Pavement. In the simulation scenarios, the driver's intention is the medium

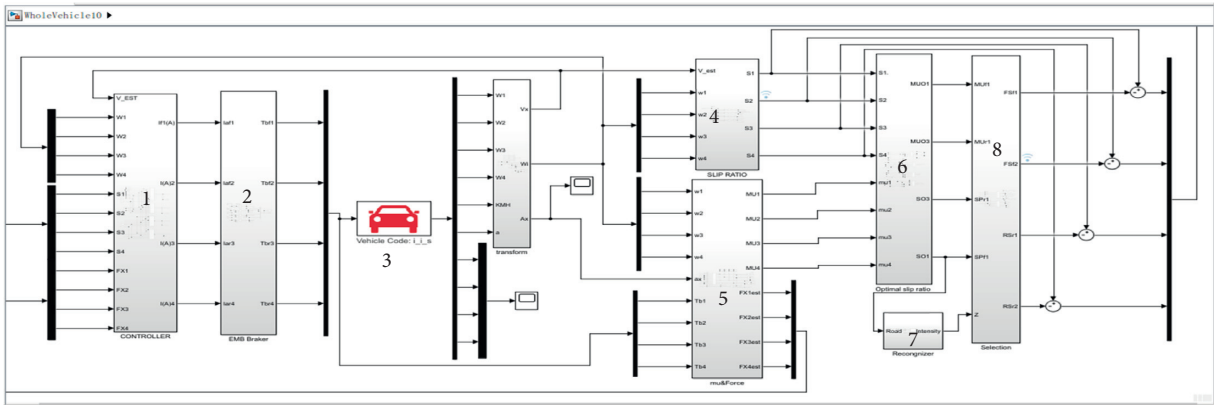

Figure 9: The structure of the simulation environment. 1: sliding mode controller. 2: EMB brake model. 3: CarSim vehicle model. 4: wheel slip rate calculation model. 5: wheel vertical load model. 6: pavement recognition model. 7: braking intention recognizer. 8: optimal braking force distribution strategy model.

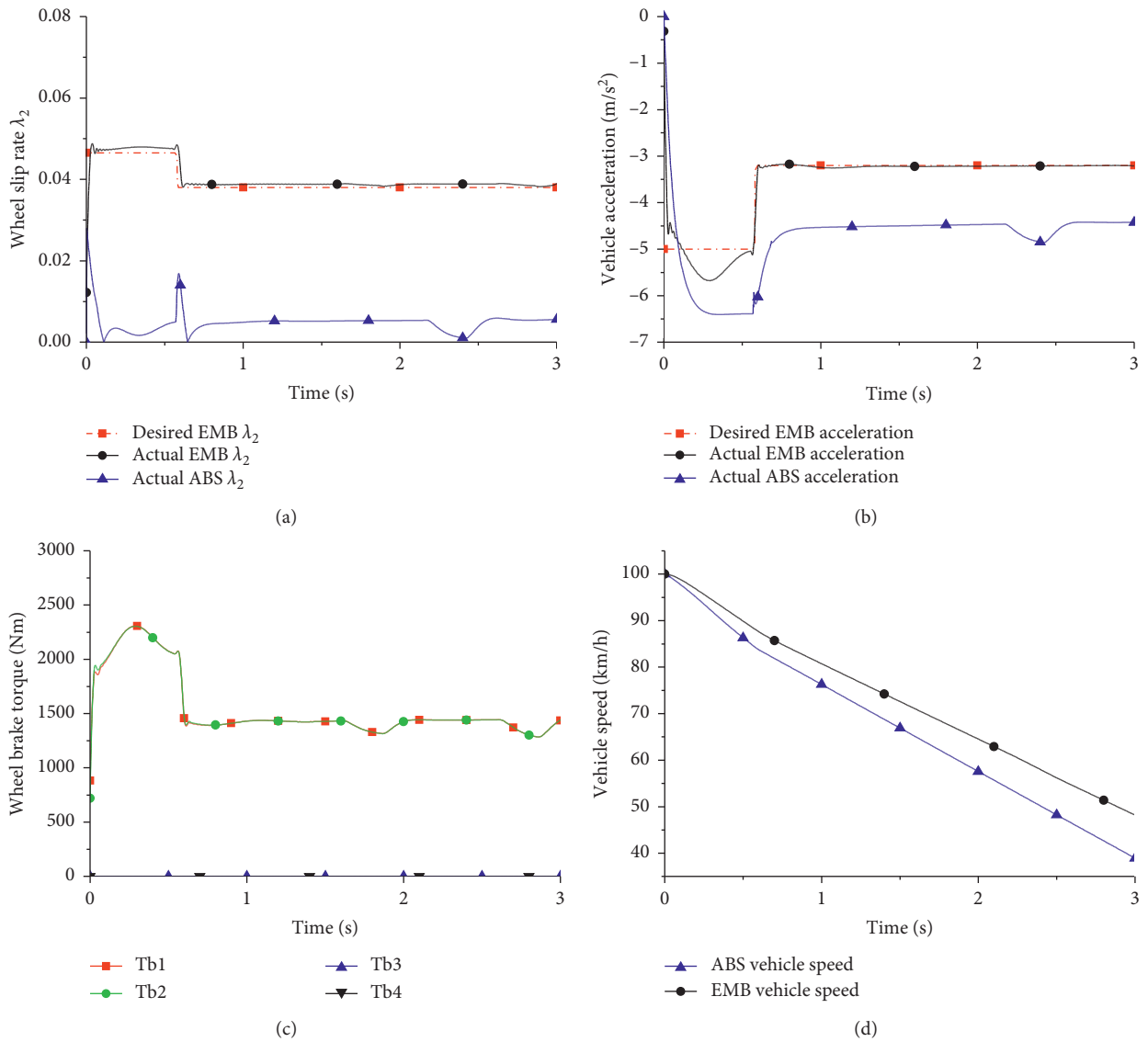

Figure 10: Medium comfort brake, switch dry asphalt pavement to wet asphalt pavement. (a) Wheel slip rate. (b) Vehicle acceleration. (c) Wheel brake torque. (d) Vehicle speed.

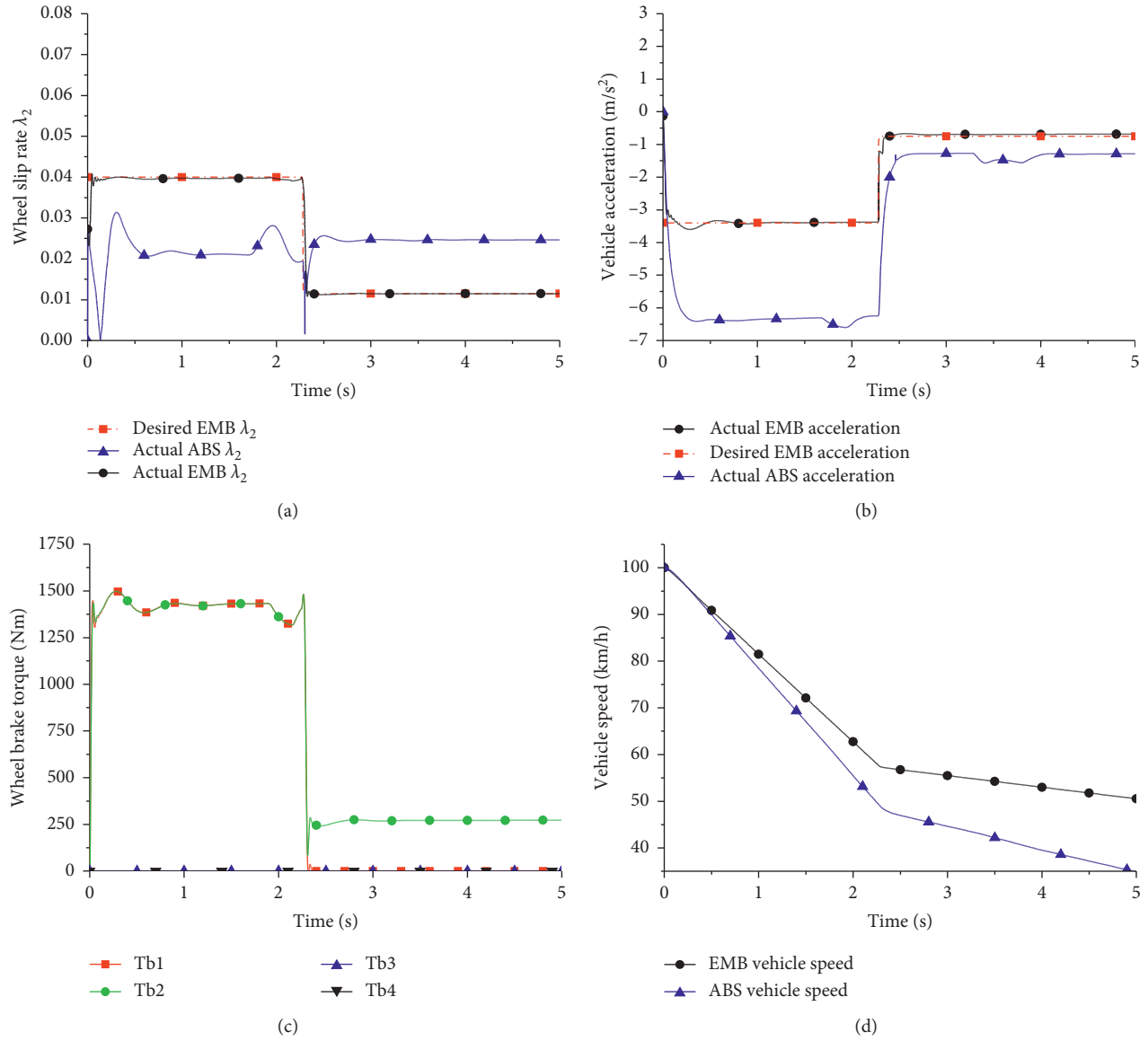

Figure 11: Medium comfort brake, switch wet asphalt pavement to snow-covered pavement. (a) Wheel slip rate. (b) Vehicle acceleration. (c) Wheel brake torque. (d) Vehicle speed.

comfort brake when $T = 0$ s, and the road surface changes from dry asphalt to snow-covered pavement at 50 meters, and the cosimulation results are shown in Figure 11.

As is shown in Figure 11, when the driver conducts the medium comfort brake on wet asphalt and snow-covered pavement, because the optimal slip rate changes with the change of the road surface and the optimal braking force distribution model will change the optimal slip rate in real time, the wheel slip rate of the EMB vehicle is changed from 0.04 to 0.01 with good adaptability, while the wheel slip rate of the ABS vehicle could not follow the desired wheel slip rate no matter on which kind of the road surface. Though the snow-covered pavement's peak adhesion coefficient is lower than other two road surfaces, the EMB vehicle also performs better on acceleration aspect, which both −0.34 g and −0.09 g are in the acceptable range. The acceleration of the ABS vehicle on the wet asphalt road is near −0.65 g which has brought the uncomfortable feeling to the passenger, but it decreases to −0.15 g which is acceptable to the passenger. The same as scenario I. (a), only the front axle brake of the EMB vehicle works in the process of braking. Compared with scenario I. (a), both conditions on wet asphalt and snow-covered pavement, the EMB vehicle has ensured the braking comfort under the premise of ensuring safety.

4.2.3. Scenario II (a) Dry Asphalt Pavement, Switch Medium Comfort Brake to Emergency Brake. In the simulation scenarios, the vehicle is running on the dry asphalt pavement all the time, the driver switches mild brake to medium comfort brake when $T = 1.5$ s, and the cosimulation results are shown in Figure 12.

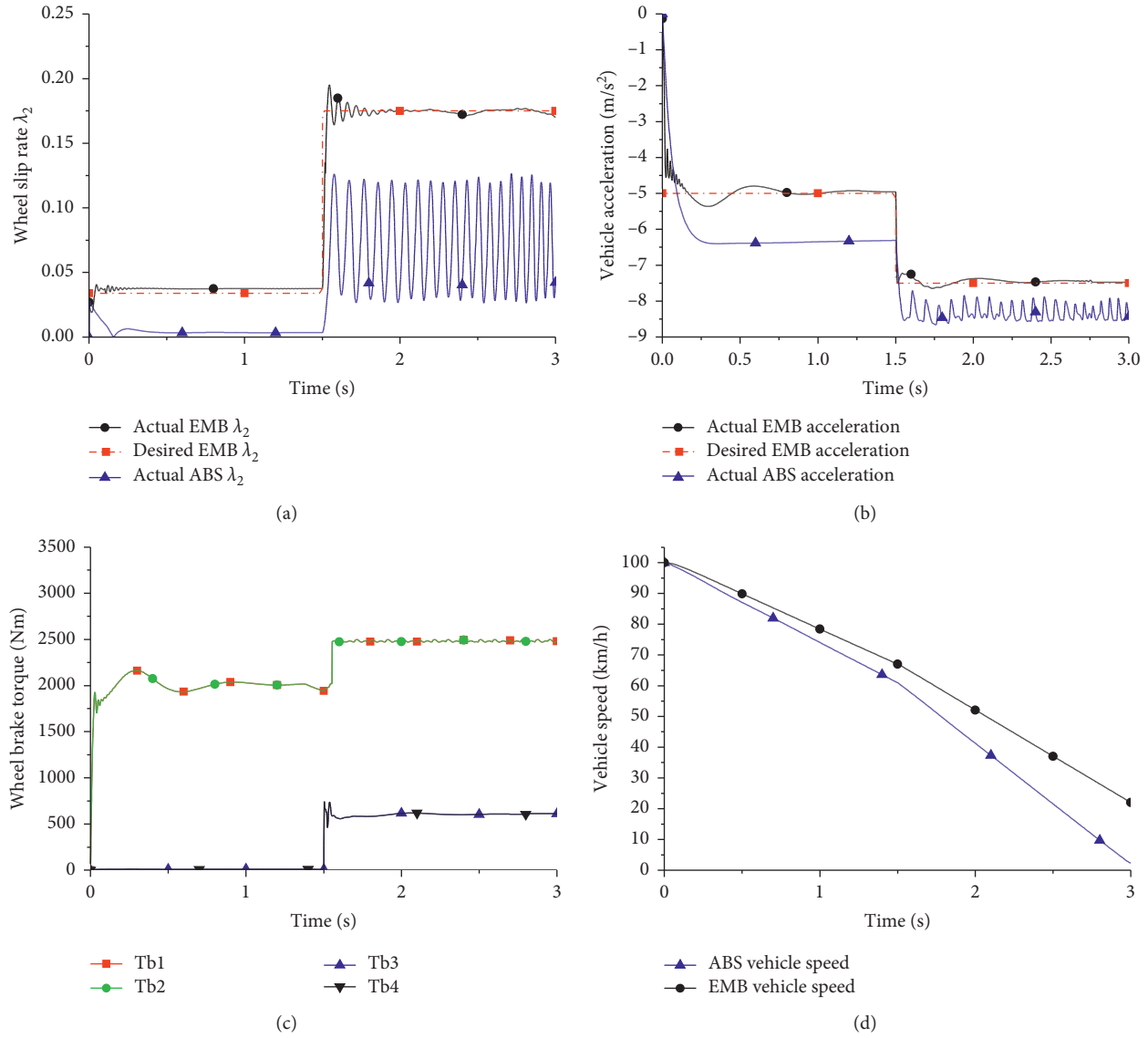

FIGURE 12: Dry asphalt pavement, switch medium comfort brake to emergency brake. (a) Wheel slip rate. (b) Vehicle acceleration. (c) Wheel brake torque. (d) Vehicle speed.

As is described above, the maximum deceleration of the vehicle when the emergency brake is applied is generally 0.75 g to 0.85 g. Figure 12 depicts the vehicle longitudinal acceleration, speed, wheel slip rate, and brake torque, respectively, when the driver switches the medium comfort brake to the emergency brake on dry asphalt pavement. The wheel slip rate of the EMB vehicle steadily is changed from 0.04 to near the optimal road slip rate 0.17, while the wheel slip rate of the ABS vehicle is controlled at the range of 0.03–0.11 due to the emergency brake. The acceleration of the EMB vehicle is kept at near −0.5 g when the medium comfort brake is conducted, and it increases to near −0.75 g 1.5s later, in which both values are in the acceptable range. The acceleration of the ABS vehicle is changed from −0.65 g to near −0.9 g 1.5 s later, in which both values are in the unacceptable range. Thus, the feeling in the EMB vehicle is better than in the ABS vehicle under the condition of ensuring vehicle safety. The same as simulation scenario I, the rear axle brake of the EMB vehicle does not work when braking intention is the medium comfort brake, but when braking intention changes to the emergency brake, the four-wheel slip rate of the EMB vehicle is set to be the road optimal slip rate 0.17, so the rear axle brake torque increased to the specified value.

4.2.4. Scenario II (b) Wet Asphalt Pavement, Switch Medium Comfort Brake to Medium Emergency Brake. In the simulation scenarios, the vehicle is running on the wet asphalt pavement all the time, the driver switches mild brake to medium comfort brake when $T = 1.5$ s, and the cosimulation results are shown in Figure 13.

As is shown in Figure 13, when the driver switches the medium comfort brake to the emergency brake on wet asphalt pavement, the wheel slip rate of the EMB vehicle is

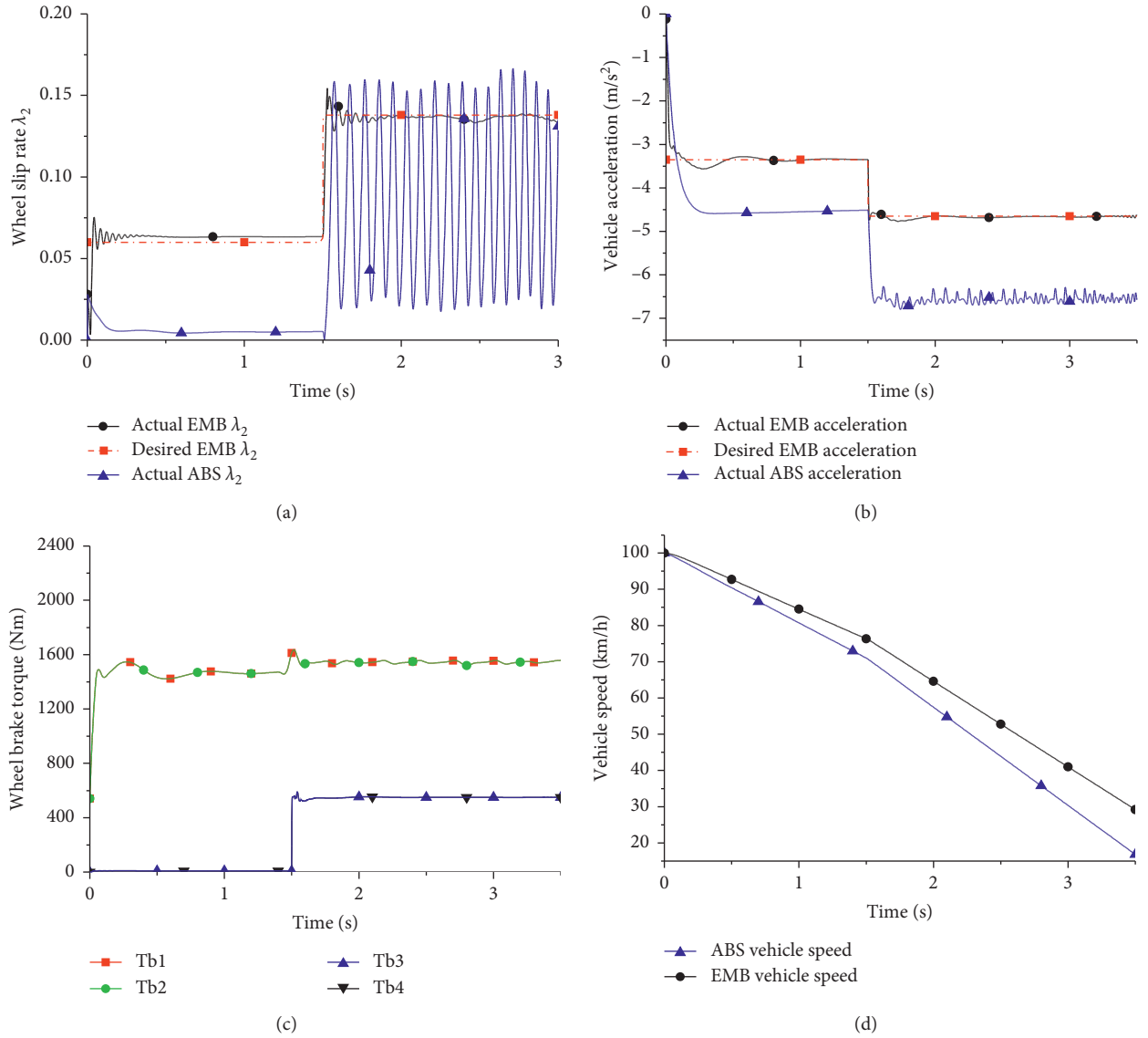

Figure 13: Wet asphalt pavement, switch medium comfort brake to emergency brake. (a) Wheel slip rate. (b) Vehicle acceleration. (c) Wheel brake torque. (d) Vehicle speed.

steadily changed from 0.06 to near-road optimal slip rate 0.1308, while the wheel slip rate of the ABS vehicle changes from near 0.01 to the range of 0.3–0.16 due to the change of intention. The EMB vehicle acceleration is changed from −0.33 g to −0.46 g, in which both values are acceptable. And the acceleration of the ABS vehicle is steadily changed from −0.45 g to −0.65 g, in which both values are on the edge of acceptance. The rear axle brake of the EMB vehicle changes the same as scenario II (a) except the specified brake torque value.

All in all, we could find that the EMB vehicle performs better than the ABS vehicle considering braking comfort. No matter which kind of condition is changed, the EMB vehicle could keep the passenger in an acceptable range. That is, the vehicle equipped with EMB can well ensure braking comfort of the vehicle equipped with the BBW system under the premise of ensuring brake safety.

5. Conclusions

In order to ensure the braking comfort of the vehicle equipped with the BBW system, a novel braking intention classification method was proposed, which included mild brake, medium comfort brake, and emergency brake. A braking intention recognizer relying on fuzzy logic was established, which could reflect driver's intention in real time; the brake pedal voltage and its change rate were taken as the recognizer input, and it outputs real-time driver's braking intention and braking intensity; an optimal brake force distribution strategy for the vehicle equipped with the BBW system based on slip rate was proposed to improve braking comfort. The vehicle dynamics model, improved sliding mode controller, and the BBW system model were constructed, respectively. The cosimulation was conducted both in Simulink and CarSim, the simulation results show

that the EMB vehicle performs better than the ABS vehicle considering braking comfort under the same condition, and the EMB vehicle braking comfort is better on wet asphalt and snow pavement than on dry asphalt pavement, and no matter which kind of road surface, the vehicle performs very well on changing intention test. The proposed braking intention classification method, braking intention recognizer, brake force distribution strategy, and sliding mode control can well ensure braking comfort of the vehicle equipped with the BBW system under the premise of ensuring brake safety. In view of this, control scheme is helpful to the control of longitudinal vibration; hence, this control algorithm concerning braking comfort will be, respectively, applied in a prototyping system and real-car experiment in the future study.

Nomenclature

a: Distance from CG to the front axle (m)
b: Distance from CG to the rear axle (m)
F_x: Wheel longitudinal ground brake force (N)
F_z: Wheel vertical load (N)
h_s: Height of center of mass of sprung mass (m)
h_{us}: Height of center of mass of unsprung mass (m)
I: Drive motor armature current (A)
I_f: Moment of inertia of the front axle (kg·m^2)
I_r: Moment of inertia of the rear axle (kg·m^2)
J: Moment of inertia of the wheel (kg·m^2)
L: Distance from the front axle to the rear axle (m)
L_b: Brake pedal opening (m)
m: Vehicle mass (kg)
m_s: Vehicle sprung mass (kg)
m_{us}: Vehicle unsprung mass (kg)
r: Wheel rolling radius (m)
r_b: Brake disc radius (m)
T_b: Wheel brake torque (N)
T_e: Drive motor electromagnetic torque (Nm)
T_f: Drive motor friction torque (Nm)
U: Output voltage of the electronic brake pedal (V)
v: Vehicle longitudinal speed (m/s)
$\dot{v}$: Vehicle longitudinal acceleration (m/s^2)
θ: Angular displacement of the brake pedal (°)
ω: Angular velocity of wheel rotation (rad/s)
$\dot{\omega}$: Angular acceleration of wheel rotation (rad/s^2)

Dimensionless
i_x: Planetary gear ratio
k_b: Brake output torque coefficient
k_t: Motor torque coefficient of the brake
k_1: Variable speed approach law coefficient
k_2: Exponential convergence law coefficient
p_h: Lead of the screw
Z: Brake intensity
η_x: Mechanical efficiency of the planetary gear mechanism
η_s: Mechanical efficiency of the ball screw
λ: Actual wheel slip ratio
λ_p: Road optimal wheel slip ratio
λ^*: Current-desired wheel slip ratio
μ: Brake force coefficient
μ_b: Brake pad friction coefficient
$\widehat{\mu}$: Actual brake force coefficient
φ: Boundary layer

Subscript
i: The number for each wheel of the vehicle.

Data Availability

The data used to support the findings of this study are available from the corresponding author upon request.

Conflicts of Interest

The authors declare that there are no conflicts of interest regarding the publication of this paper.

Acknowledgments

This research was financially supported by the National Natural Science Foundation of China (grant no. 51806114).

References

[1] S. H. Huo, L. Y. Yu, L. Y. Ma, and L. Zhang, "Ride comfort improvement in post-brake phase using active suspension," in *Proceedings of the ASME Design Engineering Technical Conference*, pp. 1–6, Boston, MA, USA, 2015.

[2] V. S. V. Satyanarayana, B. Sateesh, and N. M. Rao, "Parameters optimisation of vehicle suspension system for better ride comfort," *International Journal of Vehicle Performance*, vol. 4, no. 2, pp. 186–199, 2018.

[3] J. Lee and S. Choi, "Braking control for improving ride comfort," *MATEC Web of Conferences*, vol. 166, p. 02002, 2018.

[4] X. Y. Peng, L. He, and Y. B. Lyu, "Fuzzy sliding mode control based on vehicle slip ratio for electro-mechanical braking systems," *Journal of Central South University (Science and Technology)*, vol. 49, no. 2, pp. 360–370, 2018.

[5] S. A. Haggag and D. Abidou, "An approach to vehicle brake-by-wire optimal control tracking strategy," *SAE International Journal of Passenger Cars–Mechanical Systems*, vol. 6, no. 1, pp. 154–162, 2013.

[6] Z. C. Chen, J. Wu, J. Zhao, R. He, C. Yang, and Y. Zhang, "ABS Control Algorithm Based on Direct Slip Rate for Hybrid Brake System," in *Proceedings of the SAE Technical Paper Series*, pp. 1–8, Detroit, MI, USA, 2018.

[7] B. Wang, X. Y. Huang, J. M. Wang, X. Guo, and X. Zhu, "A robust wheel slip ratio control design combining hydraulic and regenerative braking systems for in-wheel-motors-driven electric," *Journal of the Franklin Institute*, vol. 352, no. 2, pp. 577–602, 2014.

[8] W. F. Faris, Z. BenLahcene, and F. Hasbullah, "Ride quality of passenger cars: an overview on the research trends," *International Journal of Vehicle Noise and Vibration*, vol. 8, no. 3, pp. 185–199, 2012.

[9] W. Q. Zhao, C. F. Zong, and H. Y. Zheng, "Control strategy of commercial vehicle electronic braking system based on braking comfort," *Journal of Jilin University (Engineering and Technology Edition)*, vol. 42, no. 1, pp. 22–26, 2012.

[10] P. W. Wang, L. Wang, Y. H. Li, and W. W. Guo, "Improved cooperative collision avoidance (CCA) model considering

driver comfort," *International Journal of Automotive Technology*, vol. 16, no. 6, pp. 989–996, 2015.

[11] N. Pan, L. Y. Yu, L. Zhang, J. Song, and Y. H. Zhang, "Antilock braking control in coordinated braking system considering braking comfort," *Journal of Zhejiang University (Engineering Science)*, vol. 55, no. 1, pp. 9–16, 2017.

[12] C. F. Zong, S. N. Yang, and H. Y. Zheng, "A control strategy of electronic braking system based on braking comfort," in *Proceedingsof the 2011 International Conference on Transportation, Mechanical, and Electrical Engineering*, pp. 1265–1268, IEEE, Changchun, China, 2011.

[13] H. Zheng, S. Ma, and Y. Liu, "Vehicle braking force distribution with electronic pneumatic braking and hierarchical structure for commercial vehicle," *Proceedings of the Institution of Mechanical Engineers, Part I: Journal of Systems and Control Engineering*, vol. 232, no. 4, pp. 481–493, 2018.

[14] A. Soltani, A. Bagheri, and S. Azadi, "Integrated vehicle dynamics control using semi-active suspension and active braking systems," *Proceedings of the Institution of Mechanical Engineers, Part K: Journal of Multi-Body Dynamics*, vol. 232, no. 3, pp. 314–329, 2017.

[15] G. Yin and X. Jin, "Cooperative control of regenerative braking and antilock braking for a hybrid electric vehicle," *Mathematical Problems in Engineering*, vol. 2013, Article ID 890427, 9 pages, 2013.

[16] Y. He, C. Lu, J. Shen, and C. Yuan, "Design and analysis of output feedback constraint control for antilock braking system with time-varying slip ratio," *Mathematical Problems in Engineering*, vol. 2019, Article ID 8193134, 11 pages, 2019.

[17] M. Burckhardt, *Fahrwerktechnik, Radschlupf-Regelsysteme*, pp. 39–45, Vogel Verlag, Wuerzburg, Geramny, 1993.

[18] CARSIM, *CarSim 2016 Release Note*, Mechanical Simulation Corporation, Ann Arbor, MI, USA, 2016.

[19] MATLAB, *Simulink User Guide Release R2016b*, The MathWorks, Inc., Natick, MA, USA, 2016.